




Gas sensing and photocatalytic activity of synthesized hierarchical Bi₂O₃ nanoflakes by sol–gel and nanosheets by hydrothermal method

Abhinay S. Mandawade¹, Laxmi D. Sonawane¹, Huda I. Ahemad¹, Yogesh B. Aher¹, Anil B. Gite¹, Latesh K. Nikam², Gotan H. Jain¹, Mathew D. Femi^{1,3}, Ganesh E. Patil¹, Balasaheb M. Palve^{4,*} , and Mahendra S. Shinde^{5,*}

¹ Department of Physics, SNJB's ACS College, Chandwad Nashik 423101, India

² Department of Chemistry, PDA's Annasaheb Magar College, Hadapsar, Pune 411028, India

³ Department of Physics and Astronomy, University of Nigeria, Nsukka 410001, Nigeria

⁴ Department of Physics, S.N.Arts, D.J.M. Commerce & B. N. Sarda Science College (Autonomous), Sangamner 422605, India

⁵ Department of Physics, M.J.M. ACS College, Karanjali 422208, India

Received: 17 March 2024

Accepted: 7 May 2024

© The Author(s), under exclusive licence to Springer Science+Business Media, LLC, part of Springer Nature, 2024

ABSTRACT

The research involves synthesizing hierarchical nanoflakes of bismuth oxide (Bi₂O₃) using the sol–gel (SG) method and Bi₂O₃ nanosheets through hydrothermal (HY) synthesis, with a focus on investigating their gas sensing and photocatalytic activity. The synthesized Bi₂O₃ analyzed using X-ray diffraction (XRD) techniques reveals that SG and HY are monoclinic crystal structures. Fourier-transform infrared spectroscopy (FTIR) did the functional group analysis, which shows the absorption band at 874 cm⁻¹ and 858 cm⁻¹ in typical stretching and bending vibrations characteristics. The surface morphology of synthesized Bi₂O₃ material was carried out by field emission scanning electron microscopy (FESEM), which reveals the nanosheet type morphology and one-sided arrangement like a flower by SG and HY synthesis, respectively. The gas sensing activity of Bi₂O₃ thick films was prepared by screen printing technique and examined for different gases such as H₂S, NH₃, LPG, C₂H₅OH, H₂, CH₃OH, CO₂, and Cl₂. They showed highest sensitivity to H₂S against NH₃, LPG, C₂H₅OH, H₂, CH₃OH, CO₂ and Cl₂. The catalyst Bi₂O₃ with methylene blue (MB) dye showed better photocatalytic performance of the SG method than HY synthesis.

S.I. : AMSCA: 2023 The guest editor of this special issue is Dr. Habib Pathan.

Address correspondence to E-mail: arjunpalve@gmail.com; mahen3569@rediffmail.com

<https://doi.org/10.1007/s10854-024-12739-6>

Published online: 20 May 2024

 Springer

Content courtesy of Springer Nature, terms of use apply. Rights reserved.

1 Introduction

Bismuth oxide (Bi_2O_3) is an important p-type metal oxide semiconductor that has been receiving excellent optical and electrical properties such as narrow band-gap, high refractive index, and depending on temperature [1, 2]. They have five main polymorphic forms such as α - Bi_2O_3 (monoclinic), β - Bi_2O_3 (tetragonal), γ - Bi_2O_3 (BCC), δ - Bi_2O_3 (cubic) and ω - Bi_2O_3 (triclinic) [3, 4]. These characteristics render it highly appropriate for extensive applications such as supercapacitors [5–7] Pseudo capacitor [4] antibacterial activity [8, 9] fuel cells [10] gas sensors [11–15] photocatalytic activity [16–20] etc. From the gas sensing point of view, gas sensors play a crucial role in modern society due to their essential importance as a part of an advanced technology to detect various gases at low temperatures for human safety as well as for environmental awareness [21]. Researchers are actively involved in the ongoing development of gas sensors, utilizing either metal oxide or polymer-based materials, aimed at early detection of hazardous, flammable, and toxic gases [22]. Bi_2O_3 has been mostly studied for gas-sensing. In gas sensing, the alteration of surface-electrical conductivity in the detection of explosive, hazardous, and toxic gases occurs through the adsorption of reducing or oxidizing gases onto its surface [11–13]. Many researchers tested various gases with Bi_2O_3 such as Carbon monoxide [12], Acetone and Ethanol [14], hydrogen sulfide [15], carbon dioxide [23], hydrogen [24], etc. From the catalyst degradation activity point of view, the distinctive structures of p-type Bi_2O_3 heterogeneous semiconductors make them highly effective photocatalysts, playing a crucial role in modern solid-state applications [20]. It has demonstrated significant potential for effectively treating wastewater contaminated with both organic and inorganic pollutants. In the realm of innovative water treatment technologies, advanced oxidation processes have emerged as promising methods in recent years [25]. Many researchers used various dyes for catalyst degradation with Bi_2O_3 such as methylene Blue [26], Rhodamine B [27], methyl orange [28], etc. Over the past few years, various researchers have undertaken the synthesis of Bi_2O_3 using different methods, such as sol-gel [29, 30] hydrothermal [31–33] green synthesis [33, 34] spray pyrolysis using borosilicate glass [35] solution combustion method [36] chemical method [37] chemical bath deposition (CBD) or SILAR [38–40, 44] and spin coating [41], etc. To the best of our understanding, the

SG method and HY synthesis have gained widespread popularity due to their cost-effectiveness and the use of readily available equipment, as well as their ability to operate under mild reaction conditions. These techniques play a crucial role in manipulating the morphology and crystalline structure in both approaches [42]. Therefore, the focus has been on combining the SG method and HY synthesis to comprehend how the manipulation of material morphology can influence both gas sensing and catalyst degradation activity and show better response of material [43, 44] the current study has been investigated.

In the present work, the Bi_2O_3 nanoflakes and nanosheet were successfully synthesized by using the SG method and HY synthesis and analyzed different characterization techniques, such as XRD, FTIR, FESEM-EDS, Raman, PL, and TEM-SAED. The SG method synthesized Bi_2O_3 nanoflakes determine excellent gas sensing response and catalyst degradation activity as compared to HY synthesized nanosheets when they are exposed to MB under sunlight.

2 Experimental details

2.1 Materials

Bismuth nitrate pentahydrate $\text{Bi}(\text{NO}_3)_3 \cdot 5\text{H}_2\text{O}$, Sodium hydroxide pellets (NaOH), Polyethylene Glycol 600 (PEG 600), and Nitric acid (HNO_3) were purchased from Sigma Aldrich. All chemicals were of AR grade and used without any further purification. Deionized water was used for the preparation of the solution.

2.2 Methods

2.2.1 Synthesis of Bi_2O_3 nanoflakes by SG method

For the synthesis of Bi_2O_3 , the sol-gel route was used as depicted in Fig. 1a. The 0.1 M of $\text{Bi}(\text{NO}_3)_3 \cdot 5\text{H}_2\text{O}$ was initially prepared in 50 ml distilled water by continuous stirring. Subsequently, 5 ml of PEG 600 was added as a surfactant in solution by stirring for one hour at a moderate speed of 450 rpm at room temperature. After some time, a yellowish gel formed and dried in an oven at 80 °C for 5 h. The obtained product was calcined at 500 °C in a muffle furnace for 30 min.

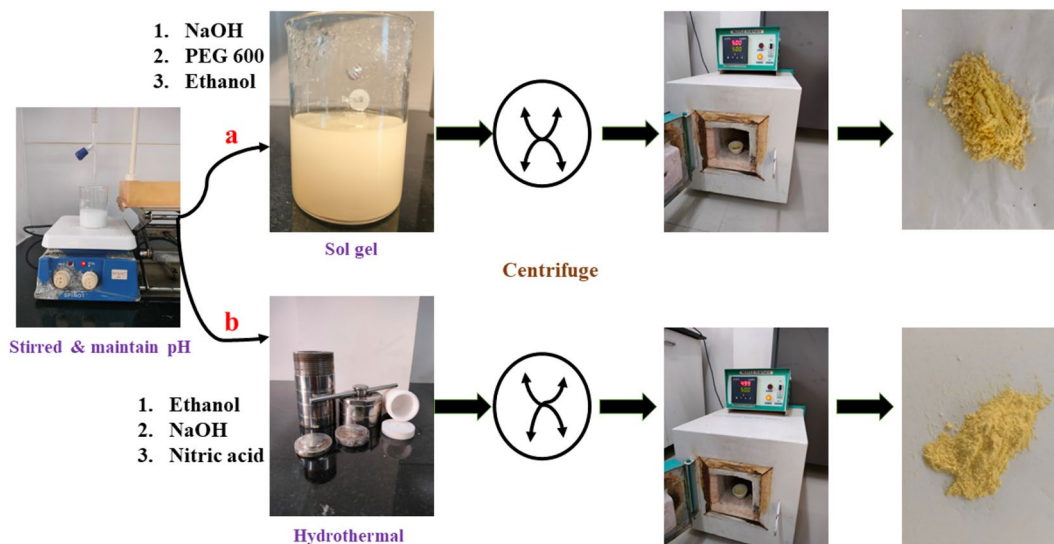


Fig. 1 Synthesis of Bi_2O_3 by a SG method and b HY synthesis

2.2.2 Synthesis of Bi_2O_3 nanosheets by HY method

For the synthesis of Bi_2O_3 , hydrothermal route has been employed, as depicted in Fig. 1b. Firstly, 0.2 M of $\text{Bi}(\text{NO}_3)_3 \cdot 5\text{H}_2\text{O}$ was added to 50 ml distilled water and HNO_3 by continuous stirring for 2 h., another beaker was prepared with 1 M NaOH solution then the solution was added dropwise by adjusting the pH of the solution. The above solution was transferred into the Teflon-lined stainless-steel autoclave maintained at a temperature 180 °C for 18 h., the mixture was cooled to room temperature. The residue was washed and dried at 120 °C, then calcined 500 °C then pure Bi_2O_3 nanosheets formed.

2.2.3 Preparation of thick films

Thick films of Bi_2O_3 sensors were prepared using the screen-printing technique. Initially, 1 gm of Bi_2O_3 material was grinded in a mortar pestle for 20 min. Then, ethyl cellulose was added to grinded Bi_2O_3 material to make a homogeneous mixture. Afterwards a binder solution (Terpentine oil, 2- butoxyethyl acetal, Butyl cellulose) was added to the mixture till the mixture turned to a homogeneous paste form. This homogeneous paste was used to prepare thick films. The thick films dried under the exposure of an iron lamp. The film was fired in a muffle furnace for

two hours at 500 °C. Then, the fabricated films were utilized for further gas-sensing application [45].

2.3 Physico-chemical characterization

The crystal structure and crystallite size of Bi_2O_3 were confirmed by X-ray Diffraction (XRD) using X-ray Source Cu $\text{K}\alpha$ Model Miniflex 600 Make Rigaku. Fourier-transform infrared spectroscopy (FTIR) was performed using IR Affinity – 1 with a diamond ATR Shimadzu Spectrometer. Field Emission Scanning Electron Microscopy (FESEM) imaging was performed using the Carl Zeiss Model Supra 55 Germany. Raman spectra were collected using the inVia Renishaw micro-Raman spectrophotometer. Photoluminescence spectra were performed using the Fluorolog (Horiba). Photoluminescence was performed using the JASCO Spectrofluorometer Model – FP-8300 WRE, and TEM images were collected using the JEOL JEM 2100 plus.

3 Result and discussion

3.1 X-ray diffraction (XRD) analysis

3.1.1 Crystallite size by Scherrer's formula

The existing crystallite size and phase of the synthesized Bi_2O_3 were determined using the X-ray

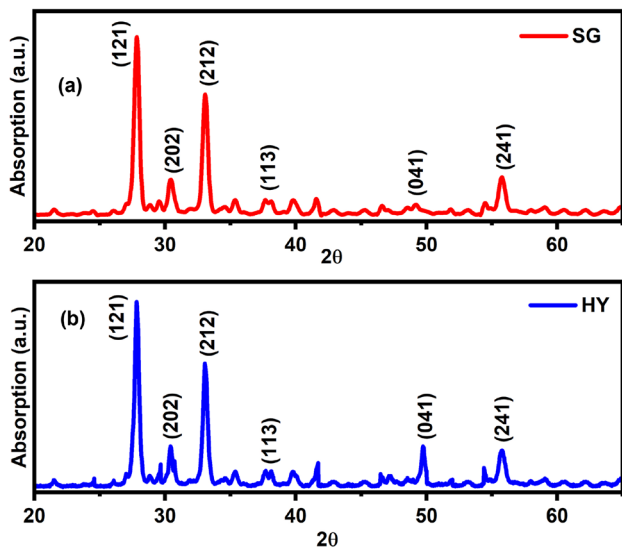


Fig. 2 XRD Pattern of Bi_2O_3 by **a** SG method and **b** HY synthesis

diffraction (XRD) technique. The XRD peaks of Bi_2O_3 material were assigned on the basis previous report [25] and JCPDS data. XRD patterns of Bi_2O_3 nanoflakes and nanosheets obtained using the SG method and HY synthesis are shown in Fig. 2a, b. The XRD pattern of the SG and HY method for Bi_2O_3 , was (121), (202), (212), (113), (041), and (241) reflection planes at 28.55° , 30.92° , 34.55° , 38.15° , 47.06° , and 54.77° respectively (JCPDS Card no: 00-041-1449). The observed crystal structure by both SG method and HY synthesis for Bi_2O_3 was Monoclinic. The average crystallite size was calculated using the Debye Scherrer formula and it was found about 15 nm and 16 nm for Bi_2O_3 by SG and HY method respectively.

3.2 Functional group analysis

The determination of the functional group present in the synthesized Bi_2O_3 was carried out by Fourier-transform infrared spectroscopy (FTIR) analysis. The FTIR spectra were recorded by in the range of $4000\text{--}400\text{ cm}^{-1}$. The nature of FTIR spectra of Bi_2O_3 synthesis by SG method and by HY method which is not the same as shown in Fig. 3a and b respectively. After the analysis of both spectra, all vibration modes are in good agreement with the literature [25, 47]. The Bi_2O_3 shows the absorption band at 1407 cm^{-1} (strong, sharp) and 1362 cm^{-1} (weak, broad) due to Bi-O stretching. In general, Bi_2O_3 shows an absorption band below 1000 cm^{-1} therefore, the absorption

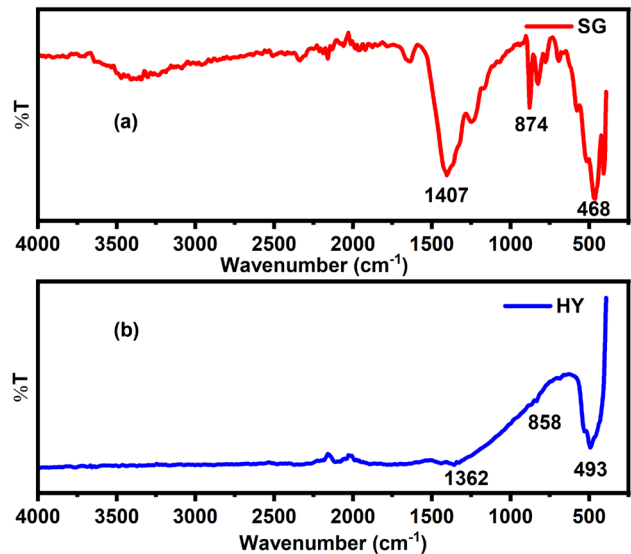


Fig. 3 FTIR Spectra of Bi_2O_3 by **a** SG method and **b** HY synthesis

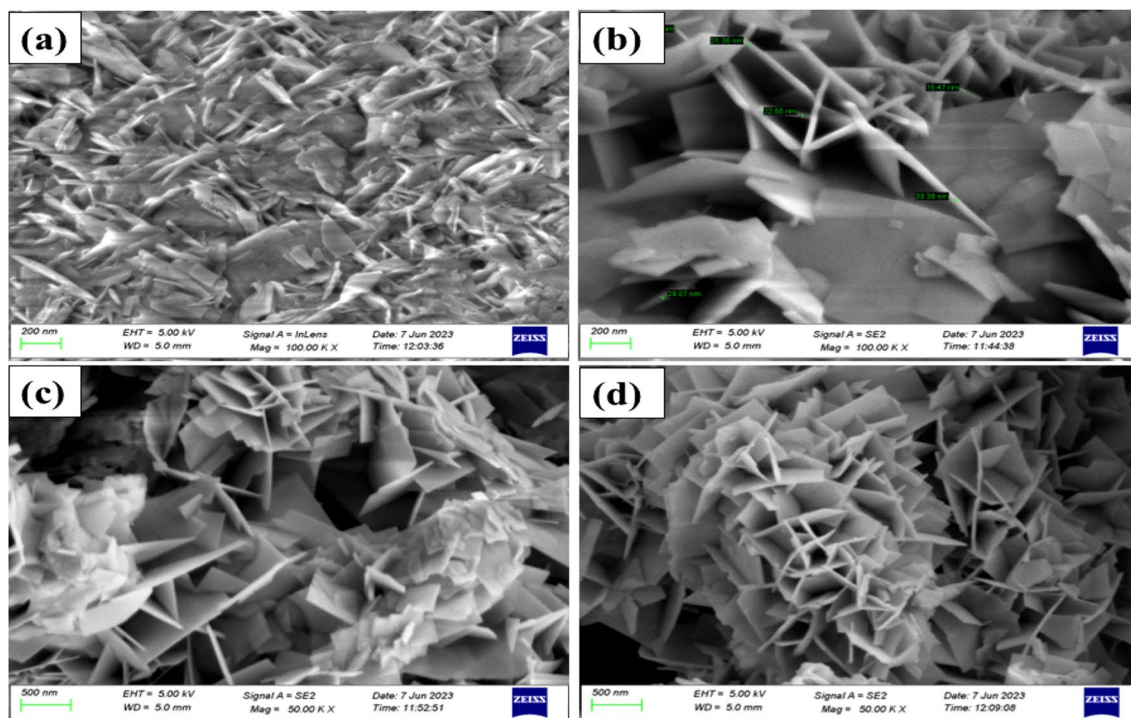
band at 874 (sharp and strong) and 858 (feeble) cm^{-1} is typical Bi-O-Bi bond stretching and bending vibrations [29].

3.3 Surface morphology studies by FESEM

The morphology of pure Bi_2O_3 synthesized by SG method and HY synthesis was analyzed by field emission scanning electron microscopy (FESEM). The FESEM images of the surface morphology of the pure Bi_2O_3 SG method are shown in Fig. 4a–d, which shows the agglomeration of particles in the form of nanoflakes and one-sided flower-like arrangement [47]. Figure 4e indicates the energy-dispersive X-ray spectroscopy (EDAX) image of pure Bi_2O_3 by SG, showing the weight and atomic% value of Bi and O elements, which have K and M shells, respectively. The morphology exposed plane layers in Fig. 5a, c and d. Figure 5b clearly shows an irregular distribution with nanosheets-like morphology [50], showing the number of holes present over the surface of pure Bi_2O_3 HY synthesis. The elemental analysis of composition was examined by EDAX, which confirms that oxygen is a more deficient SG method than HY synthesis in Fig. 5e.

3.4 Raman analysis

Figure 6a demonstrates peaks at 126, 209, 277, 315, 448, and 535 cm^{-1} , and Fig. 6b demonstrates peaks at 118,



07-06-2023 | S5 | Area 1 | Selected Area 1

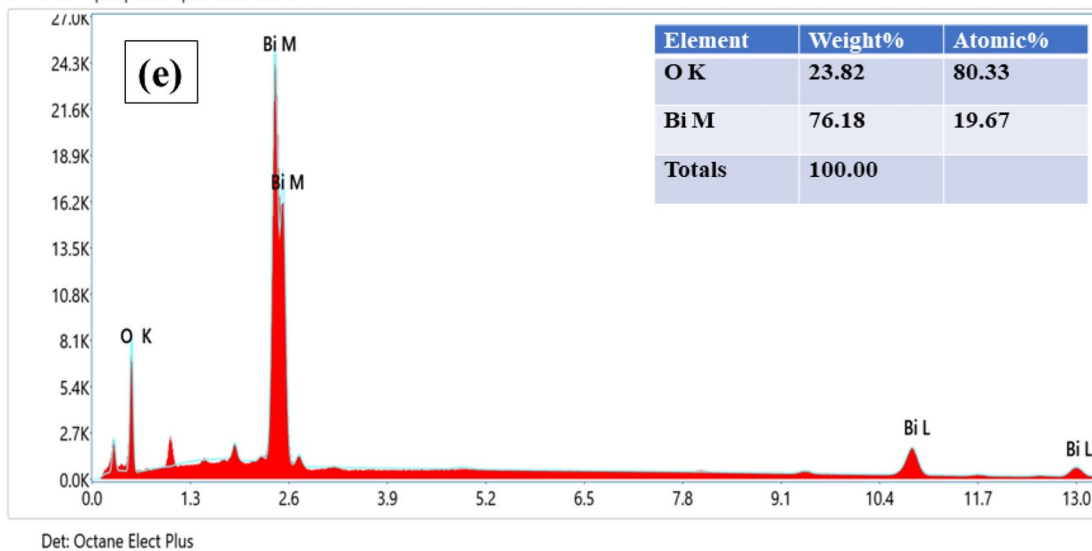


Fig. 4 a–d The FESEM images of Bi_2O_3 at different magnifications of the SG method and e EDAX spectra

152, 184, 210, 302, 411, and 439 cm^{-1} for pure Bi_2O_3 SG and HY method respectively, which is similar to the Raman spectrum of Bi_2O_3 in previous studies [33, 48, 49]. The nature of Raman spectra observed for Bi_2O_3 synthesized by SG method and HY synthesis is not the same indicating structural difference and depicting $\leftarrow\text{-Bi}_2\text{O}_3$ in SG and the mixture of $\leftarrow\text{-Bi}_2\text{O}_3$ and $\leftarrow\text{-Bi}_2\text{O}_3$ crystalline forms in HY sample. The assignment of

bands [51–53] observed in SG and HY samples are given in following Table 1.

3.5 Photoluminescence (PL) study

Figure 7a shows the Photoluminescence spectra (PL) of SG method and Fig. 7b PL spectra of HY synthesis excited by 480 nm radiation. The PL spectra are

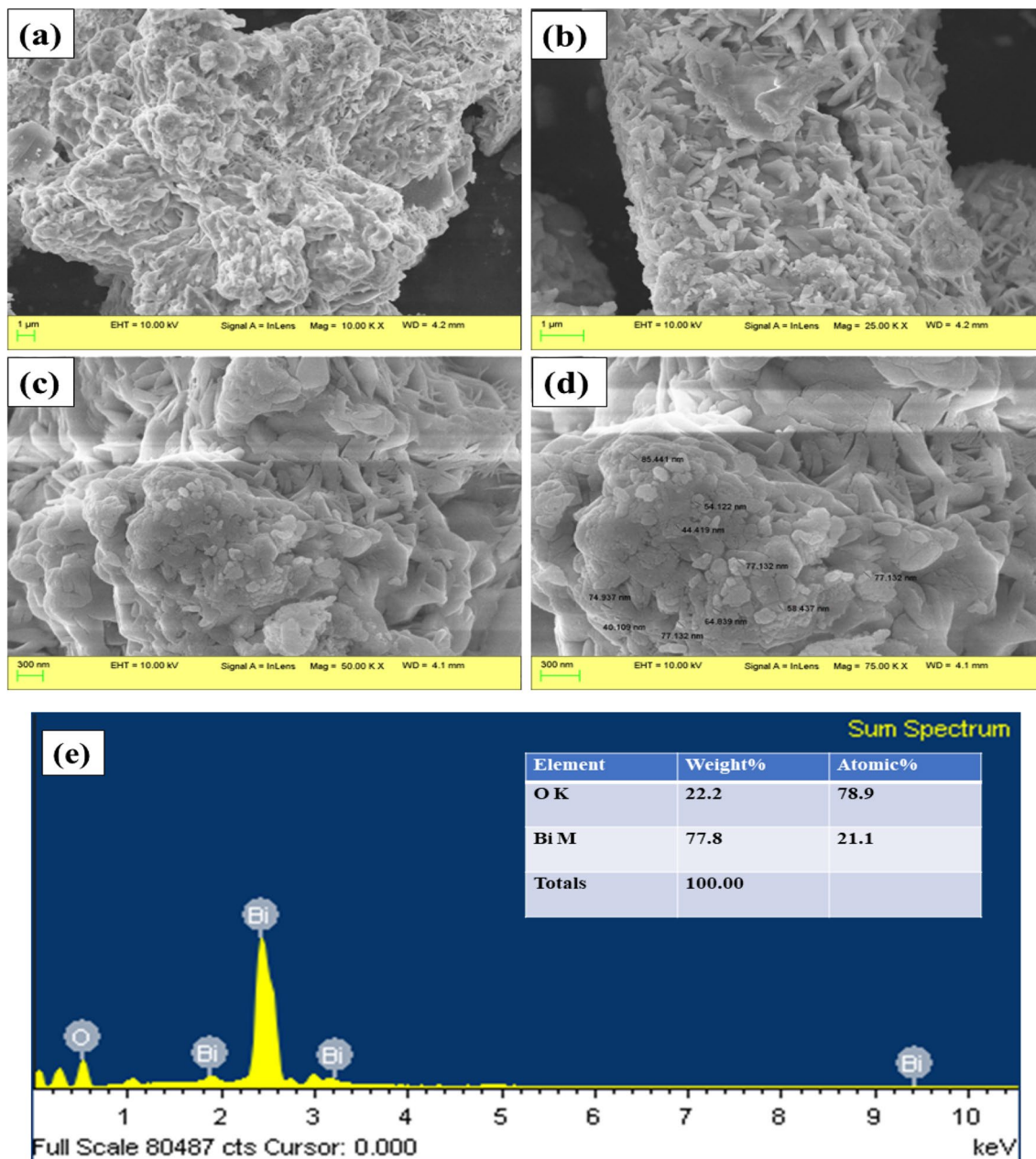


Fig. 5 a–d The FESEM images of Bi_2O_3 at different magnifications of HY synthesis and e EDAX spectra of Bi_2O_3

related to the transfer behavior of the photo-induced electrons and holes [17]. In Fig. 7a, three peaks 529 nm, 657 nm, and 791 nm, can be seen, meaning three recombined semiconductors. In Fig. 7b, Three peaks 529 nm, 657 nm, and 790 nm, can be seen, meaning three recombined semiconductors [54]. The PL spectra of Bi_2O_3 synthesized by SG method and HY synthesis seem to be exactly similar and have low intense isolated emission peaks at 529 nm, 657 nm, and 790 nm and attributed to Bi^{3+} ions [55]. Low-intensity peak

indicates a lower recombination rate of the electron–hole pair. This is favorable for photocatalysis.

3.6 TEM analysis

Figure 8a and b shows the TEM images of SG method and HY synthesis. The size distribution in Fig. 8c and

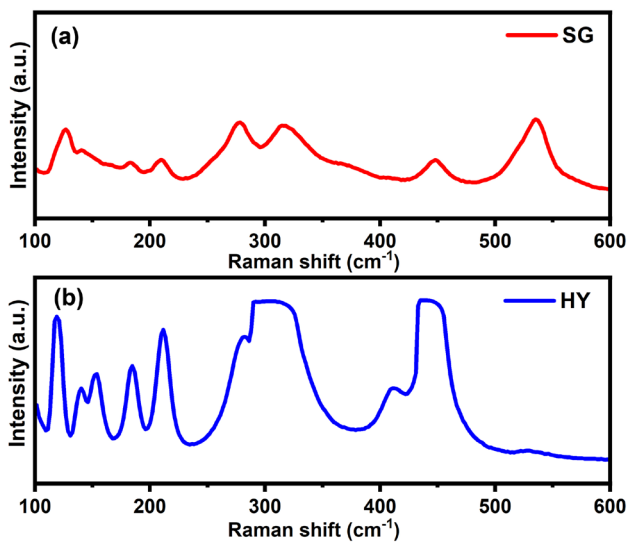


Fig. 6 Raman spectra of Bi₂O₃: **a** SG method, **b** HY synthesis

d of the Bi₂O₃ SG method and HY synthesis samples have average particle sizes of 28.50 nm and 60.56 nm in Fig. 8e and f. The lattice spacing of 0.361 and 0.513 nm corresponds to the (121) and (212) planes, respectively. Figure 8g and h shows the SAED patterns based on JCPDS file no 00-041-1449 corresponding to the monoclinic structure.

3.6.1 Gas sensing mechanisms

The schematic representation of the Bi₂O₃ sensor for H₂S sensing is represented in Fig. 9a. In air, the oxygen molecules adsorb on the sensor surface and gain electrons from the conduction band of Bi₂O₃ material, forming oxygen ions. This conduction band electron is responsible for the depletion region of certain sensor surfaces. In Fig. 9b, During the H₂S gas molecules adsorb at the sensor surface and react with oxygen ions. The electron is released back to the sensor material, reducing the depletion region width at the sensor’s surface [15].

As explained earlier, the remarkable gas sensing characteristics of Bi₂O₃, fabricated through the SG and HY methods, can be attributed to factors such as reduced particle size, an abundance of oxygen vacancies, and an increased porous structure. In our investigation, the interaction between H₂S and oxygen species emerges sequentially. Initially, oxygen is adsorbed onto the material’s surface, where it appropriates free electrons, transforming oxygen anions [56].

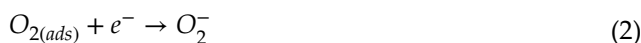


Table 1 Raman Active vibrational modes (a) SG method and (b) HY synthesis

SG	HY	Assignment	References
	118	<- Bi ₂ O ₃ due to Ag symmetry	[48]
126		©- Bi ₂ O ₃	
	152	<- Bi ₂ O ₃	
	184	<- Bi ₂ O ₃	[49]
209	210	<- Bi ₂ O ₃	
277 medium broad symmetric	277 medium broad shoulder	©- Bi ₂ O ₃	
315 medium broad symmetric	315 Broad and strong asymmetric shape	©- Bi ₂ O ₃	
	411 medium broad	<- Bi ₂ O ₃	
448 Broad and weak	439 Broad and strong	©- Bi ₂ O ₃	
535		©- Bi ₂ O ₃	
620		Weak broad vibrational band, Associated with structural disorder in crystal due to non-thermodynamic growth condition as well as due to δ cubic phase	[51]

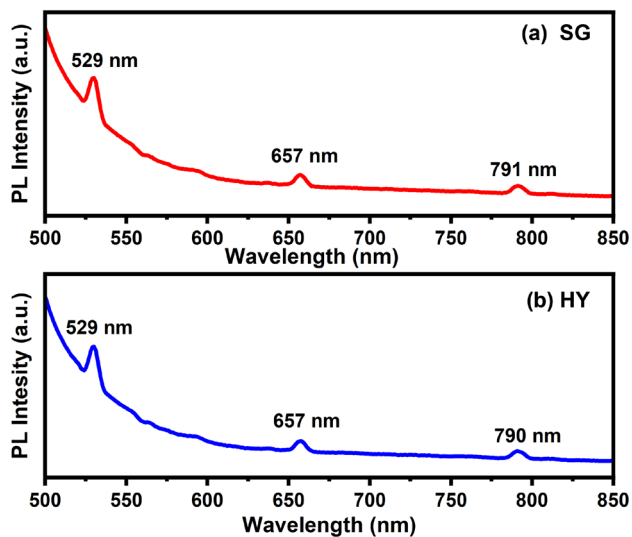
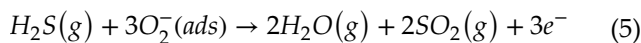


Fig. 7 PL spectra of a Bi_2O_3 : **a** SG method, **b** HY synthesis



The recovery process involves the reactivation of the sensor surface as it is exposed to ambient conditions, during which the adsorption of oxygen species plays a crucial role in restoring the sensor functionality after removing H_2S .



From Fig. 10, The capacity of a sensor to respond to a particular gas in the presence of other gases is known as selectivity. A series of gases were used to demonstrate the room-temperature gas-sensing performance of the as-obtained Bi_2O_3 Nanosensors. To investigate the selectivity SG method and HY synthesis of Bi_2O_3 sensors were exposed to eight gases, including Hydrogen sulfide (H_2S), ammonia (NH_3), LPG, Ethanol ($\text{C}_2\text{H}_5\text{OH}$), Hydrogen (H_2), Methanol (CH_3OH), Carbon dioxide (CO_2) and Chlorine (Cl_2) and their responses were measured at various temperatures ranging from room temperature to 450°C for 100 ppm gas concentration. A good sensitivity response for H_2S is compared with other target gases. This study reveals that the sensor has a specific affinity for H_2S gas and exhibits the highest response [56].

Bi_2O_3 was exposed to different concentrations of H_2S gas response in the previous literature [57]. From Fig. 11a, sol-gel thick films show 76.99% sensitivity of H_2S gas at an operating temperature 100°C with a gas concentration of 100 ppm. In Fig. 11b, hydrothermal thick films show 68.59% sensitivity to H_2S gas at an operating temperature of 100°C with a gas concentration 100 ppm. The time interval of operating temperature is 50°C during the measurement of gas response. For measurement of H_2S gas sensitivity, the temperature range varied from room temperature to 450°C . The gas sensitivity of the prepared Bi_2O_3 thick film was calculated using an equation,

$$S(\%) = \frac{R_a - R_g}{R_a} \times 100$$

where, R_a = Resistance of Bi_2O_3 thick film sensor in the presence of air, R_g = Resistance of Bi_2O_3 thick film sensor in the presence of targeted gas.

From Fig. 12, The concentration effect of H_2S gas on the prepared (a) SG method and (b) we investigated HY synthesis, the concentration effect of H_2S gas on the sensor for different concentrations from 10 to 150 ppm at 100°C and 100°C [15].

Figure 13a shows that the thick film sensor was kept at 100°C , the optimum temperature for the SG method. Then, H_2S gas was injected using a syringe in the glass dome of the gas sensing system for measurement of a response time is 32 s, whereas recovery time was 63 s to Bi_2O_3 thick film sensor for H_2S gas at a concentration of 100 ppm. Along with Fig. 13b, HY synthesis at 100°C optimum temperature response time is 43 s, whereas recovery time was 71 s to Bi_2O_3 thick film sensor for H_2S gas at a concentration of 100 ppm.

4 Photocatalytic experiment

4.1 Mechanism of degradation

The photocatalytic mechanism is shown in Fig. 14. The Bi_2O_3 photocatalyst first absorbed the light to generate a free electron-hole pair on the surface. Then, the electron reacted with oxygen to generate free electron-hole pairs on the surface. Meanwhile, the holes

Fig. 8 TEM – SAED of Bi_2O_3 (**a, c, e, g**) by SG method and **b, d, f, h** HY synthesis (**a, b**) Low resolution of TEM images (**c, d**) particle size histogram (**e, f**) high-resolution TEM images (**g, h**) SAED pattern

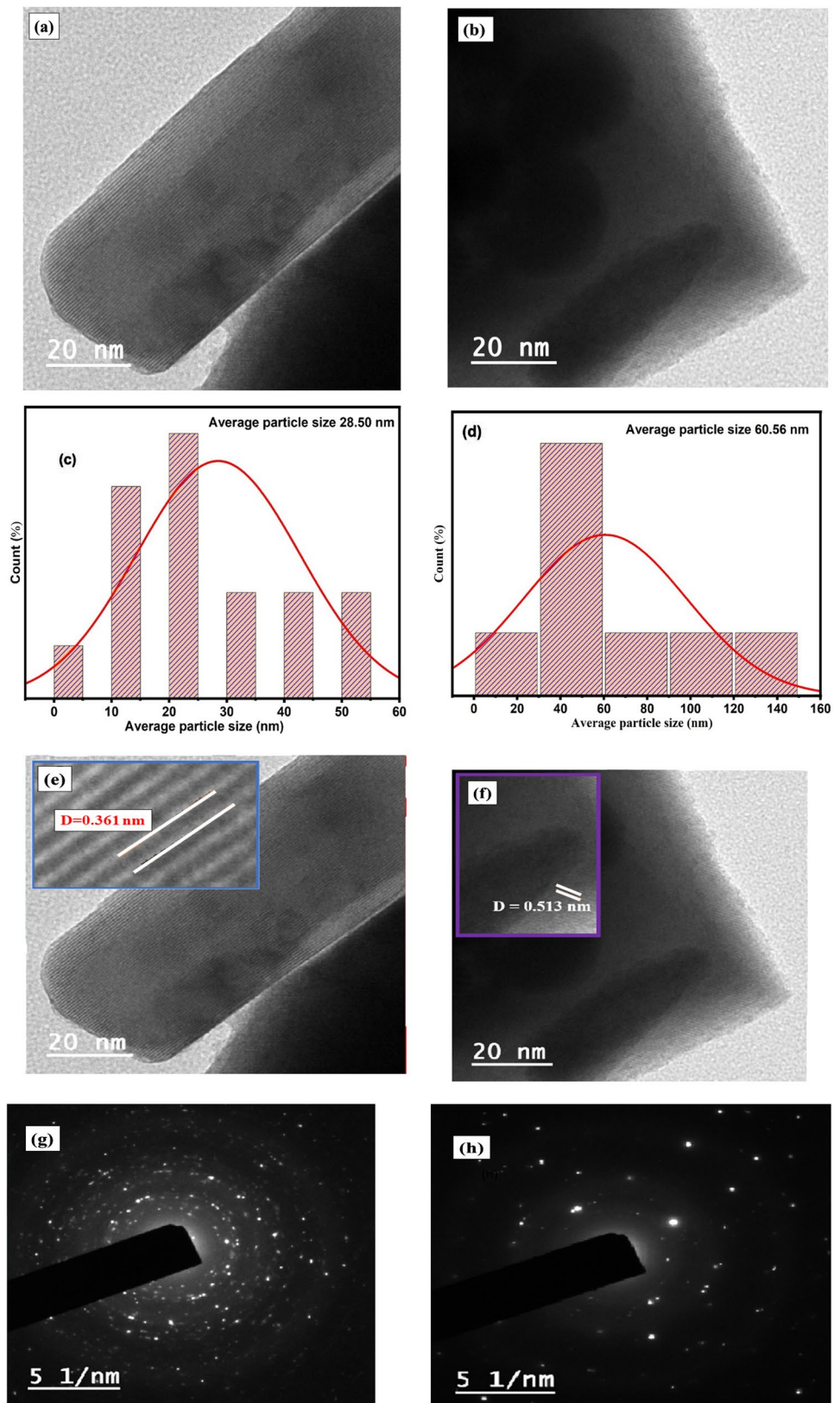
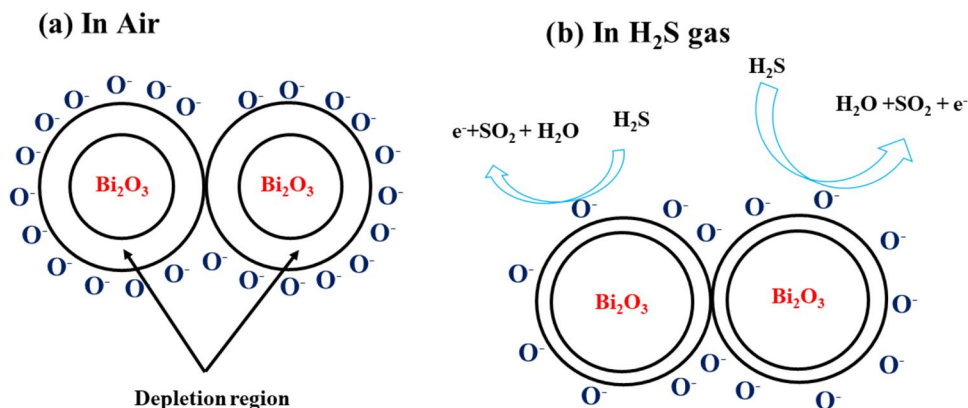
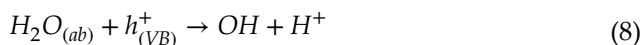
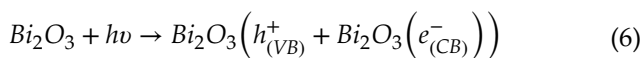


Fig. 9 Schematic of H₂S sensing mechanism for Bi₂O₃ sensor: **a** oxidation, **b** reduction



redox with H₂O to produce OH radicals, leading to the degradation of MB dye.



To study photocatalytic degradation efficiency of synthesis of Bi₂O₃ by Fig. 15a SG method and Fig. 15b HY synthesis using methylene blue (MB) used as a model dye. For this perseverance, the mixture of 100 mL of 10 ppm aqueous dye solution and 10 mg of catalyst was magnetically stirred for 30 min in the dark to achieve adsorption–desorption equilibrium between the photocatalyst and dye the solution. The mixture is then kept under sunlight between 12.00–02.00 pm with continuous and constant stirring in May. Sun meter DSM measures the intensity of the sun. The reaction mixture was withdrawn and preserved in a test tube covered with black paper. The preserved samples were centrifuged to remove the catalyst and take UV–vis spectra. The concentration of dyes has been determined in terms of absorbance at 664 nm. A kinetics study was performed to interpret the efficiency of the catalyst.

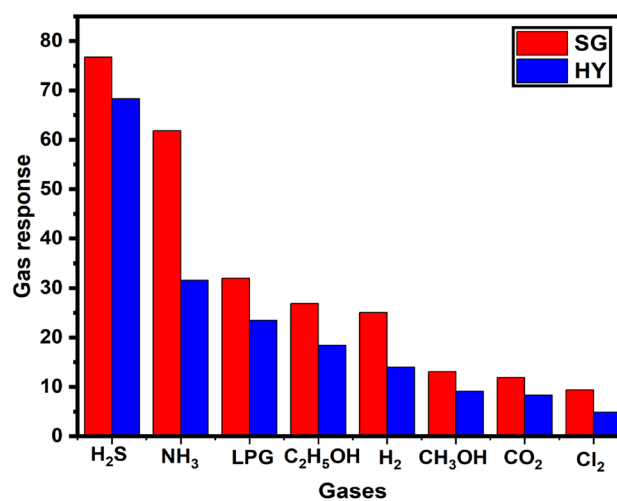


Fig. 10 Highest Selectivity for H₂S gas against all other tested gases of Bi₂O₃

4.2 Photocatalytic degradation of MB solution

Methylene Blue, a phenothiazine derivative, is reported to be a carcinogenic and toxic compound used as a dye in textile, printing, and food industries. Various methods such as adsorption, ozonation, extraction, ion flotation, Fenton process, oncolysis, ultrafiltration, etc. have been used to remove dyes from polluted water, but have limitations. The various advanced oxidation process has been employed to degrade organic pollutants, which produces harmless products like H₂O and CO₂. Photocatalytic degradation of organic pollutants using nanomaterial such as oxide, and sulfide is being employed by many researchers, and they are attempting to increase the

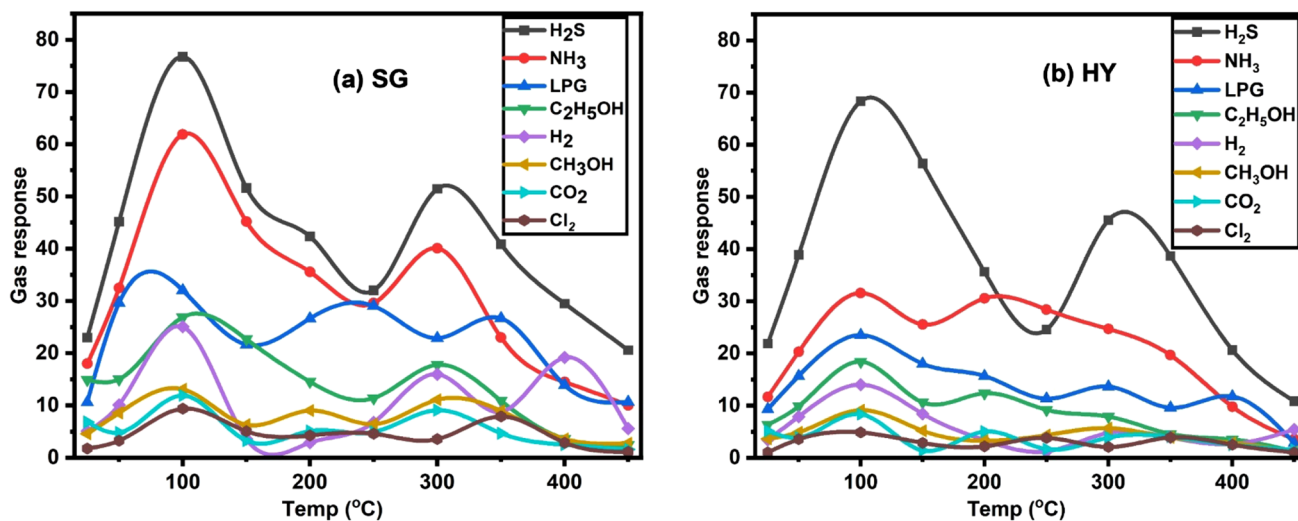


Fig. 11 H₂S sensing response at different temperatures for a SG method and b HY synthesis

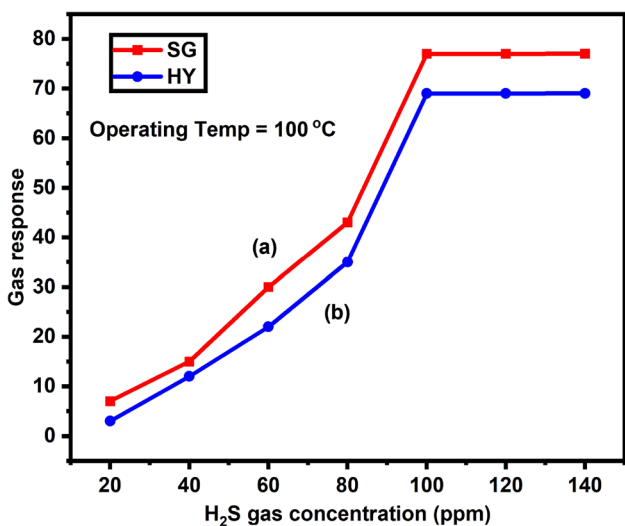


Fig. 12 H₂S gas concentration (ppm) at operating temp: a SG—100 °C, b HY—100 °C

photocatalytic efficiency of degradation [58]. This study aims to determine the efficiency of Bi₂O₃ nano-material for the degradation of organic pollutants such as dyes and hazardous chemicals. The degradation of methylene blue using Bi₂O₃ synthesized by two different methods is shown in Fig. 15a and b. The Bi₂O₃ synthesized by SG method and HY synthesis have $\lambda_{max} = 664 \text{ nm}$ indicating that MB degraded in 120 min. under the direct exposure of sunlight radiation.

4.3 Kinetic study

Figure 16a illustrates the photodegradation of MB dye by Bi₂O₃ catalyst using pseudo-first-order Langmuir – Hinshelwood kinetic equation [47]. The kinetic degradation of MB depicts that the photocatalytic efficiency of Bi₂O₃ synthesized by the SG method is more than synthesized by HY synthesis with rate constant 0.02706 min⁻¹ and 0.01889 min⁻¹ respectively. The following equation expresses the reaction,

$$\ln(A_0/A) = K_r t$$

where, K_r is the rate constant of the reaction, A_0 is the initial concentration of MB (0 min), A is the final concentration of MB, t is time in minute.

Figure 16b curves illustrate, linear nature passes through the origin of the $\ln \ln(A_0/A)$ graph Vs time indicating photocatalytic degradation of MB by Bi₂O₃. The confirmation of diffusion-controlled activity across the entire concentration range supports the appropriateness of employing linear fitting as identified in the calibration curve [59]. The photodegradation rate of MB dye Table 2 (SG method) and Table 3 (HY synthesis) was 95.73% and 90.22% following 120 min of sunlight exposure, as illustrated in Fig. 16c.

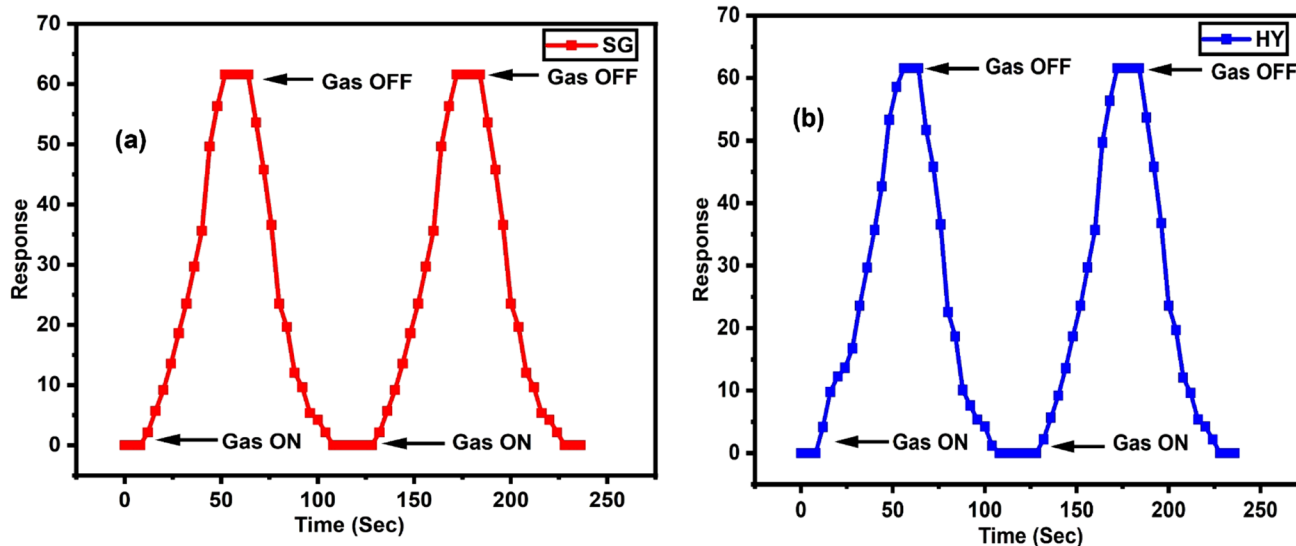


Fig. 13 Response and recovery time of H₂S gas for a Bi₂O₃ thick film for SG method and b Bi₂O₃ thick film for HY synthesis

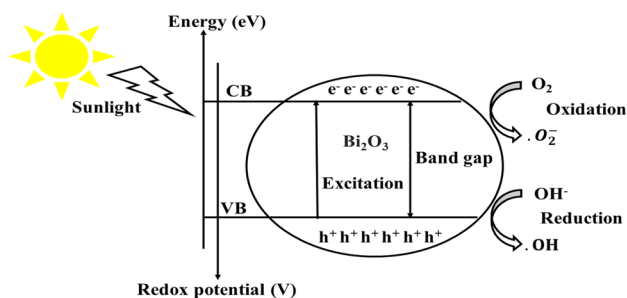


Fig. 14 The mechanism of MB dye in decomposition of Bi₂O₃

5 Conclusion

The successfully synthesized bismuth oxide (Bi₂O₃) material in hierarchical nanoflakes and nanosheet form by sol-gel (SG) and hydrothermal (HY) methods by using bismuth nitrate pentahydrate as a precursor. The results obtained from both methods were analyzed and compared. Characterization results revealed the monoclinic structures. The average crystallite size was found to vary between 15 and 16 nm. These nano metal oxides show excellent gas sensing

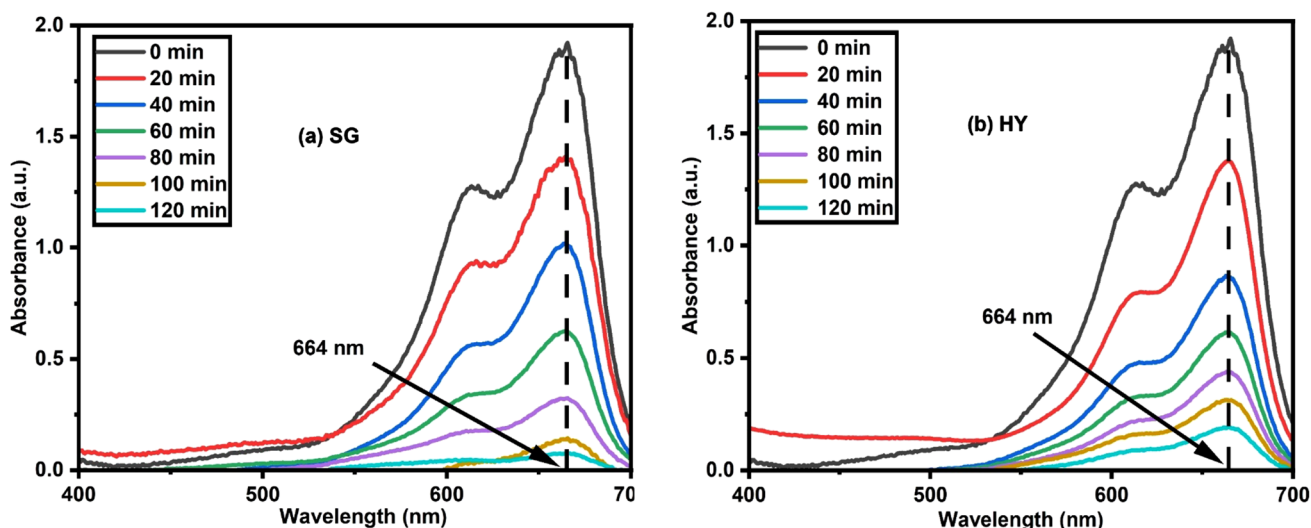


Fig. 15 The change in absorption spectra of MB using Bi₂O₃ as a catalyst prepared by a SG method, b HY synthesis

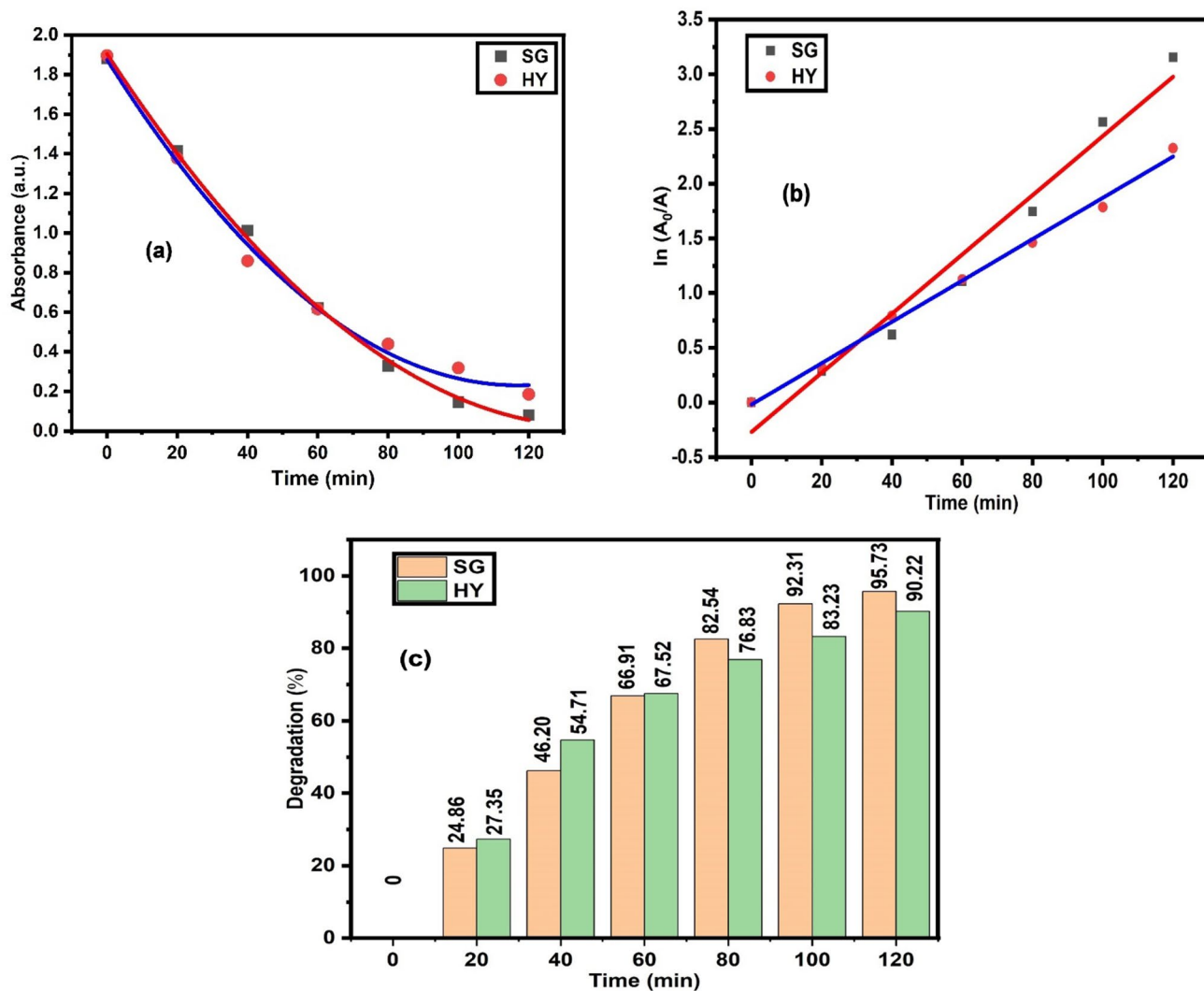


Fig. 16 a absorbance spectra (b) $\ln(A_0/A)$ versus the irradiation time for SG method and HY synthesis. (c) % degradation of MB dye for SG method and HY synthesis

Table 2 Rate constant and kinetic studies of Bi_2O_3 by SG method for MB decolorization under sunlight irradiation

Time (in min)	A	A_0/A	$\ln(A_0/A)$	% D
0	1.8828	1	0	0
20	1.4146	1.330977	0.285913	24.86722
40	1.0128	1.859005	0.620041	46.20778
60	0.6229	3.022636	1.106129	66.91629
80	0.3286	5.729763	1.745674	82.54727
100	0.1447	13.01175	2.565853	92.31464
120	0.0803	23.44707	3.154746	95.73508

Table 3 Rate constant and kinetic studies of Bi_2O_3 by HY synthesis for MB decolorization under sunlight irradiation

Time (in min)	A	A_0/A	$\ln(A_0/A)$	% D
0	1.896	1	0	0
20	1.3773	1.376606	0.319621	27.35759
40	0.8586	2.208246	0.792199	54.71519
60	0.6158	3.078922	1.124579	67.5211
80	0.4393	4.315957	1.462319	76.83017
100	0.3179	5.96414	1.785765	83.23312
120	0.1854	10.22654	2.324986	90.22152

performance and high efficiency in photodegradation under sunlight irradiation of the methylene blue dye. Thus, we conclude that the synthesized Bi_2O_3 are highly effective material for significant gas sensing activity and photodegradation application. SG can produce materials with high surface area and porosity, providing more active sites for gas molecules and enhancing sensitivity. These factors collectively contribute to the SG methods superior performance in gas sensing and photocatalytic activity compared to HY synthesis.

Acknowledgements

The author (ASM) thanks the Baburaoji Gholap College, Pune, for the XRD, UV, and FTIR facilities. The authors also thank Savitribai Phule Pune University Pune (Department of Physics) for providing Raman and PL characterization facilities. “Authors are thankful to the Department of Science and Technology for providing research facilities under the FIST programme (Project No: SR/FIST-415/2018)”. The authors thank the Mastertech lab Thane (W) for providing FESEM- EDAX (Mapping) and TEM facilities. The authors are also grateful to the Principal of SNJB ACS College for providing all the required facilities.

Author contributions

ASM—writing, original draft, funding acquisition. LDS—data curation. HIA—software. YBA—formal analysis. ABG—review and editing. LKN—data curation. GHJ—supervision. MDF—review editing. GEP—review and editing. BMP—review and editing. MSS—supervision, visualization and conceptualization.

Funding

This work was supported by the Mahajyoti (MJRF-fellowship2022_2573) Institute of Maharashtra for the Research fellowship grant.

Data availability

All data generated or analyzed during this study are presented in the main manuscript.

Declarations

Conflict of interest All authors read and approved the final manuscript. The authors declare that they have no conflict of interest.

Research involving human participants or animals This manuscript does not contain any studies with human participants or animals performed by any of the authors.

References

1. K. Szostak, P. Ostaszewski, J. Pulit-Prociak et al., Bismuth oxide nanoparticles in drug delivery systems. *Pharm. Chem. J.* **53**, 48–51 (2019). <https://doi.org/10.1007/s11094-019-01954-9>
2. X. Gou, R. Li, G. Wang et al., Room-temperature solution synthesis of Bi_2O_3 nanowires for gas sensing application. *Nanotechnology* **20**, 495501 (2009). <https://doi.org/10.1088/0957-4484/20/49/495501>
3. Y. Lu, Y. Zhao, J. Zhao et al., Induced aqueous synthesis of metastable β - Bi_2O_3 microcrystals for visible-light photocatalyst study. *Crystal Growth Des.* **15**(3), 1031–1042 (2015). <https://doi.org/10.1021/cg500792v>
4. X. Huang, W. Zhang, Y. Tan et al., Facile synthesis of rod-like Bi_2O_3 nanoparticles as an electrode material for pseudocapacitors. *Ceram. Int.* **42**, 2099–2105 (2016). <https://doi.org/10.1016/j.ceramint.2015.09.157>
5. M. Pooladi, M.M. Zerafat, Controlled micro/mesoporous carbon aerogel structure as a template for Bi_2O_3 nanoparticles/rods to improve the performance of asymmetric supercapacitors. *J Energy Storage.* **42**, 102994 (2021). <https://doi.org/10.1016/j.est.2021.102994>
6. L. Gurusamy, S. Anandan, N. Liu et al., Synthesis of a novel hybrid anode nanoarchitecture of Bi_2O_3 /porous-RGO nanosheets for high-performance asymmetric supercapacitor. *J. Electroanal. Chem.* **856**, 113489 (2020). <https://doi.org/10.1016/j.jelechem.2019.113489>
7. A. Deepi, G. Sriresh, A.S. Nesaraj, Electrochemical performance of Bi_2O_3 decorated graphene nano composites for supercapacitor applications. *Nano-Struct. Nano-Objects* **15**, 10–16 (2018). <https://doi.org/10.1016/j.nano.2018.03.003>
8. A.M.N. Jassim, S.A. Farhan, J.A.S. Salman et al., Study the antibacterial effect of bismuth oxide and tellurium nanoparticles. *Int. J. Chem. Biomol. Sci.* **1**, 81–84 (2015)

9. S. Aggrawal, I. Chauhan, P. Mohanty, Immobilization of Bi₂O₃ nanoparticles on the cellulose fibers of paper matrices and investigation of its antibacterial activity against *E. coli* in visible light. *Mater. Express* **5**, 429–436 (2015). <https://doi.org/10.1166/mex.2015.1260>
10. E. Antolini, Carbon supports for low-temperature fuel cell catalysts. *Appl. Catal. B* **88**, 1–24 (2009). <https://doi.org/10.1016/j.apcatb.2008.09.030>
11. M. Ahila, E. Subramanian, D. Pathinettam Padiyan, Optical properties of Codium tomentosum seaweed like Bi₂O₃ nanostructure and its gas-sensing activity. *Ionics (Kiel)*. **24**, 1827–1839 (2018). <https://doi.org/10.1007/s11581-017-2331-3>
12. Y. Hanifehpour, M. Abdolmaleki, Magnetic, optical and carbon monoxide gas sensing properties of facile solid state fabricated Bi₂O₃ nanomaterial. *Nanochem. Res.* **8**, 71–77 (2023). <https://doi.org/10.22036/ncr.2023.01.007>
13. S.P. Subin David, S. Veeralakshmi, J. Sandhya et al., Room temperature operatable highly sensitive toluene gas sensor using chemiresistive Ag/Bi₂O₃ nanocomposite. *Sens. Actuators B* **320**, 128410 (2020). <https://doi.org/10.1016/j.snb.2020.128410>
14. A. Moumen, D. Zappa, N. Poli et al., Catalyst—assisted vapor liquid solid growth of α -Bi₂O₃ nanowires for acetone and ethanol detection. *Sens. Actuators B* **346**, 130432 (2021). <https://doi.org/10.1016/j.snb.2021.130432>
15. K.D. Bhalerao, Y.T. Nakate, S.P. Choudhury et al., Synthesis, characterizations, and hydrogen sulfide gas sensing application of BiO_x (x = 1, 1.5) nanostructures. *Int. J. Hydrogen Energy* **48**, 840–848 (2023). <https://doi.org/10.1016/j.ijhydene.2022.09.235>
16. T.O. Ajiboye, O.A. Oyewo, D.C. Onwudiwe, The performance of bismuth-based compounds in photocatalytic applications. *Surf. Interfaces* **23**, 100927 (2021). <https://doi.org/10.1016/j.surfin.2021.100927>
17. G. Viruthagiri, P. Kannan, Visible light mediated photocatalytic activity of cobalt doped Bi₂O₃ nanoparticles. *J. Market. Res.* **8**, 127–133 (2019). <https://doi.org/10.1016/j.jmrt.2017.06.011>
18. D. Sánchez-Martínez, I. Juárez-Ramírez, L.M. Torres-Martínez et al., Photocatalytic properties of Bi₂O₃ powders obtained by an ultrasound-assisted precipitation method. *Ceram. Int.* **42**, 2013–2020 (2016). <https://doi.org/10.1016/j.ceramint.2015.10.007>
19. A. Hernández-Gordillo, J.C. Medina, M. Bizarro et al., Photocatalytic activity of enlarged microrods of α -Bi₂O₃ produced using ethylenediamine-solvent. *Ceram. Int.* **42**, 11866–11875 (2016). <https://doi.org/10.1016/j.ceramint.2016.04.109>
20. W. Raza, M.M. Haque, M. Muneer et al., Synthesis, characterization and photocatalytic performance of visible light induced bismuth oxide nanoparticle. *J. Alloys Compd.* **648**, 641–650 (2015). <https://doi.org/10.1016/j.jallcom.2015.06.245>
21. J.S. Lee, O.S. Kwon, S.J. Park, E.Y. Park et al., Fabrication of ultrafine metal-oxide-decorated carbon nanofibers for DMMP sensor application. *ACS Nano* **5**, 7992–8001 (2011). <https://doi.org/10.1021/nn202471f>
22. N.D. Hoa, N. Van Quy, H. Jung et al., Synthesis of porous CuO nanowires and its application to hydrogen detection. *Sens Actuators B* **146**, 266–272 (2010). <https://doi.org/10.1016/j.snb.2010.02.058>
23. A.R. Choudhary, S.A. Waghuley, In situ Bi₂O₃-loaded polypyrrole nanocomposites for carbon dioxide gas sensing. *Iran. Polym. J. (English Edn)*. **28**, 933–941 (2019). <https://doi.org/10.1007/s13726-019-00754-y>
24. P.V. Shinde, B.G. Ghule, S.F. Shaikh et al., Microwave-assisted hierarchical bismuth oxide worm-like nanostructured films as room-temperature hydrogen gas sensors. *J. Alloys Compd.* **802**, 244–251 (2019). <https://doi.org/10.1016/j.jallcom.2019.06.182>
25. S.D. Khairnar, V.S. Shrivastava, Photocatalytic degradation of chlorpyrifos and methylene blue using α -Bi₂O₃ nanoparticles fabricated by sol–gel method. *SN Appl. Sci.* **1**, 762 (2019). <https://doi.org/10.1007/s42452-019-0761-4>
26. M.S. Devi, S. Abinaya, T. Maiyalagan et al., Nanorods of α -Bi₂O₃ for photocatalytic degradation of methylene blue. *Mater Today Proc.* **50**, 2840–2846 (2020). <https://doi.org/10.1016/j.matpr.2020.08.813>
27. K.K. Bera, R. Majumdar, M. Chakraborty et al., Phase control synthesis of A B and A/B Bi₂O₃ hetero-junction with enhanced and synergistic photocatalytic activity on degradation of toxic dye, Rhodamine-B under natural sunlight. *J. Hazard. Mater.* **352**, 182–191 (2018). <https://doi.org/10.1016/j.jhazmat.2018.03.029>
28. S.A. Hosseini, R. Saeedi, Photocatalytic degradation of methyl orange on Bi₂O₃ and Ag₂O-Bi₂O₃ nano photocatalysts. *Bull. Chem. React. Eng. Catal.* **12**(1), 96–105 (2017). <https://doi.org/10.9767/brec.12.1.623.96-105>
29. Y. Astuti, B.M. Listyani, L. Suyati et al., Bismuth oxide prepared by sol-gel method: variation of physicochemical characteristics and photocatalytic activity due to difference in calcination temperature. *Indonesian J. Chem.* **21**(1), 108–117 (2021). <https://doi.org/10.22146/ijc.53144>
30. M.M. Patil, V.V. Deshpande, S.R. Dhage et al., Synthesis of bismuth oxide nanoparticles at 100°C. *Mater. Lett.* **59**, 2523–2525 (2005). <https://doi.org/10.1016/j.matlet.2005.03.037>

31. X. Guo, T.T. Liang, M. Rager et al., Low-temperature controlled synthesis of novel bismuth oxide (Bi₂O₃) with microrods and microflowers with great photocatalytic activities. *Mater. Lett.* **228**, 427–430 (2018). <https://doi.org/10.1016/j.matlet.2018.06.058>
32. A.M. Abdulkarem, A.A. Aref, A. Abdulhabeeb et al., Synthesis of Bi₂O₃/Cu₂O nanoflowers by hydrothermal method and its photocatalytic activity enhancement under simulated sunlight. *J. Alloys Compd.* **560**, 132–141 (2013). <https://doi.org/10.1016/j.jallcom.2013.01.134>
33. P.B. Chouke, K.M. Dadure, A.K. Potbhare et al., Biosynthesized δ-Bi₂O₃ nanoparticles from *Crinum viviparum* flower extract for photocatalytic dye degradation and molecular docking. *ACS Omega* **7**, 20983–20993 (2022). <https://doi.org/10.1021/acsomega.2c01745>
34. N. Motakef-Kazemi, M. Yaqoubi, Green synthesis and characterization of bismuth oxide nanoparticle using mentha pulegium extract. *Iran. J. Pharm. Res.* **19**(2), 70–79 (2020). <https://doi.org/10.22037/ijpr.2019.15578.13190>
35. P. Gopinath, R. Chandiramouli, Effect of annealing on spray deposited Bi₂O₃ thin film. *Res. J. Pharm. Biol. Chem. Sci.* **4**(3), 8–14 (2013)
36. J. La, Y. Huang, G. Luo et al., Synthesis of bismuth oxide nanoparticles by solution combustion method. *Part Sci. Technol.* **31**, 287–290 (2013). <https://doi.org/10.1080/02726351.2012.727525>
37. P.V. Shinde, B.G. Ghule, N.M. Shinde et al., Room-temperature successive ion transfer chemical synthesis and the efficient acetone gas sensor and electrochemical energy storage applications of Bi₂O₃ nanostructures. *New J. Chem.* **42**, 12530–12538 (2018). <https://doi.org/10.1039/c8nj02079e>
38. P.V. Shinde, N.M. Shinde, S.F. Shaikh et al., Room-temperature synthesis and CO₂-gas sensitivity of bismuth oxide nanosensors. *RSC Adv.* **10**, 17217–17227 (2020). <https://doi.org/10.1039/d0ra00801j>
39. Y. Wang, L. Jiang, D. Tang et al., Characterization of porous bismuth oxide (Bi₂O₃) nanoplates prepared by chemical bath deposition and post annealing. *RSC Adv.* **5**, 65591–65594 (2015). <https://doi.org/10.1039/c5ra09949h>
40. S.M. Pawar, B.S. Pawar, J.H. Kim et al., Recent status of chemical bath deposited metal chalcogenide and metal oxide thin films. *Curr. Appl. Phys.* **11**, 117–161 (2011). <https://doi.org/10.1016/j.cap.2010.07.007>
41. H. Soon Min. (2019). PREPARATION OF THIN FILMS BY SILAR AND SPIN COATING METHOD. Preparation of cobalt selenide thin films View project Thin film View project Sachindranath Das Jadavpur University. 165–172 <https://www.researchgate.net/publication/338736850>.
42. M. Lal, P. Sharma, L. Singh et al., Photocatalytic degradation of hazardous Rhodamine B dye using sol-gel mediated ultrasonic hydrothermal synthesized ZnO nanoparticles. *Results Eng.* **17**, 100890 (2023). <https://doi.org/10.1016/j.rineng.2023.100890>
43. S. Gupta, A.M. Divakaran, K. Awasthi, M. Kumar, CO₂ gas sensing properties of Na₃BiO₄-Bi₂O₃ mixed oxide nanostructures. *Environ. Sci. Pollut. Res.* **30**(28), 71933–9 (2023)
44. P.L. Meena, A.K. Surela et al., Bi₂O₃ nanoparticles: phyto-genic synthesis, effect of calcination on physico-chemical characteristics and photocatalytic activity. *Mater. Res. Innov.* (2023). <https://doi.org/10.1080/14328917.2023.2258469>
45. U. Jagannath Tupe, A. Vitthal Patil, M. Sarvottam Zambare et al., Stannous oxide thick film nanosensors design by screen printing technology: structural, electrical parameters and H₂s gas detection study. *Article history. Mat. Sci. Res. India* **18**(1), 66–74 (2021). <https://doi.org/10.13005/msri/180108>
46. M.W. Kim, B. Joshi, E. Samuel et al., Highly nanotextured β-Bi₂O₃ pillars by electrostatic spray deposition as photoanodes for solar water splitting. *J. Alloys Compd.* **764**, 881–889 (2018). <https://doi.org/10.1016/j.jallcom.2018.06.047>
47. S.D. Khairnar, A.N. Kulkarni, S.G. Shinde et al., Synthesis and characterization of 2-D La-doped Bi₂O₃ for photocatalytic degradation of organic dye and pesticide. *J. Photochem. Photobiol.* **6**, 100030 (2021). <https://doi.org/10.1016/j.jpap.2021.100030>
48. M. Jalalah, M. Faisal, H. Bouzid et al., Comparative study on photocatalytic performances of crystalline α- and β-Bi₂O₃ nanoparticles under visible light. *J. Ind. Eng. Chem.* **30**, 183–189 (2015). <https://doi.org/10.1016/j.jiec.2015.05.020>
49. T. Selvamani, S. Anandan, L. Granone et al., Phase-controlled synthesis of bismuth oxide polymorphs for photocatalytic applications. *Mater Chem Front.* **2**, 1664–1673 (2018). <https://doi.org/10.1039/c8qm00221e>
50. P. Rani, R. Dahiya, M. Bulla et al., Hydrothermal-assisted green synthesis of reduced graphene oxide nanosheets (rGO) using lemon (Citrus Limon) peel extract. *Mater. Today Proc.* (2023). <https://doi.org/10.1016/j.matpr.2023.04.419>
51. R.J. Bexch, W.B. Whiter, Vibrational spectra of bismuth oxide and the sillenite-structure bismuth oxide derivatives*, n.d. **34A**, 505–514.
52. N.V. Skorodumova, A.K. Jonsson, M. Herranen, M. Strømme, G.A. Niklasson, B. Johansson, S.I. Simak,

- Random conductivity of δ -Bi₂O₃ films. *Appl. Phys. Lett.* **86**, 241910–241913 (2005). <https://doi.org/10.1063/1.1948516>
53. O. Depablos-Rivera, A. Martínez, S.E. Rodil, Interpretation of the Raman spectra of bismuth oxide thin films presenting different crystallographic phases. *J. Alloys Compd.* **853**, 157245 (2021). <https://doi.org/10.1016/j.jallcom.2020.157245>
54. Q. Zhang, B. Huang, P. Wang et al., Synthesis and photocatalytic properties of one-dimensional composite Bi₂O₃ - Bi₂CrO₆ Nanowires. *Int. J. Photoenergy* (2012). <https://doi.org/10.1155/2012/461291>
55. M. Malligavathy, S. Iyyapushpam, S.T. Nishanthi et al., Remarkable catalytic activity of Bi₂O₃/TiO₂ nanocomposites prepared by hydrothermal method for the degradation of methyl orange. *J. Nanoparticle Res.* **19**, 144 (2017). <https://doi.org/10.1007/s11051-017-3806-x>
56. Z.H. Mahmoud, O.D. Abdalstar, N. Sabah, Semiconductor metal oxide nanoparticles: a review for the potential of H₂S gas sensor application. *Earthline J. Chem. Sci.* **4**, 199–208 (2020). <https://doi.org/10.34198/ejcs.4220.199208>
57. Monica Jaiswal, Robin Kumar et. al., Rapid and reversible detection of trace amounts of H₂S in air and packaged food using a biogenic bismuth oxide nanorod colorimetric sensor. *Sensors and Actuators B: Chemical.* **381** (2023). Doi: <https://doi.org/10.1016/j.snb.2023.133395>
58. Z.Z. Vasiljevic, M.P. Dojcinovic, J.D. Vujancevic et al., Photocatalytic degradation of methylene blue under natural sunlight using iron titanate nanoparticles prepared by a modified sol-gel method: Methylene blue degradation with Fe₂TiO₅. *R Soc Open Sci.* **7**, 200708 (2020). <https://doi.org/10.1098/rsos.200708>
59. K.B. Kusuma, M. Manju, C.R. Ravikumar, N. Raghavendra et al., Photocatalytic degradation of Methylene Blue and electrochemical sensing of paracetamol using Cerium oxide nanoparticles synthesized via sonochemical route. *Applied Surface Science Advances.* **11**, 100304 (2022). <https://doi.org/10.1016/j.apsadv.2022.100304>

Publisher's Note Springer Nature remains neutral with regard to jurisdictional claims in published maps and institutional affiliations.

Springer Nature or its licensor (e.g. a society or other partner) holds exclusive rights to this article under a publishing agreement with the author(s) or other rightsholder(s); author self-archiving of the accepted manuscript version of this article is solely governed by the terms of such publishing agreement and applicable law.

Terms and Conditions

Springer Nature journal content, brought to you courtesy of Springer Nature Customer Service Center GmbH (“Springer Nature”).

Springer Nature supports a reasonable amount of sharing of research papers by authors, subscribers and authorised users (“Users”), for small-scale personal, non-commercial use provided that all copyright, trade and service marks and other proprietary notices are maintained. By accessing, sharing, receiving or otherwise using the Springer Nature journal content you agree to these terms of use (“Terms”). For these purposes, Springer Nature considers academic use (by researchers and students) to be non-commercial.

These Terms are supplementary and will apply in addition to any applicable website terms and conditions, a relevant site licence or a personal subscription. These Terms will prevail over any conflict or ambiguity with regards to the relevant terms, a site licence or a personal subscription (to the extent of the conflict or ambiguity only). For Creative Commons-licensed articles, the terms of the Creative Commons license used will apply.

We collect and use personal data to provide access to the Springer Nature journal content. We may also use these personal data internally within ResearchGate and Springer Nature and as agreed share it, in an anonymised way, for purposes of tracking, analysis and reporting. We will not otherwise disclose your personal data outside the ResearchGate or the Springer Nature group of companies unless we have your permission as detailed in the Privacy Policy.

While Users may use the Springer Nature journal content for small scale, personal non-commercial use, it is important to note that Users may not:

1. use such content for the purpose of providing other users with access on a regular or large scale basis or as a means to circumvent access control;
2. use such content where to do so would be considered a criminal or statutory offence in any jurisdiction, or gives rise to civil liability, or is otherwise unlawful;
3. falsely or misleadingly imply or suggest endorsement, approval, sponsorship, or association unless explicitly agreed to by Springer Nature in writing;
4. use bots or other automated methods to access the content or redirect messages
5. override any security feature or exclusionary protocol; or
6. share the content in order to create substitute for Springer Nature products or services or a systematic database of Springer Nature journal content.

In line with the restriction against commercial use, Springer Nature does not permit the creation of a product or service that creates revenue, royalties, rent or income from our content or its inclusion as part of a paid for service or for other commercial gain. Springer Nature journal content cannot be used for inter-library loans and librarians may not upload Springer Nature journal content on a large scale into their, or any other, institutional repository.

These terms of use are reviewed regularly and may be amended at any time. Springer Nature is not obligated to publish any information or content on this website and may remove it or features or functionality at our sole discretion, at any time with or without notice. Springer Nature may revoke this licence to you at any time and remove access to any copies of the Springer Nature journal content which have been saved.

To the fullest extent permitted by law, Springer Nature makes no warranties, representations or guarantees to Users, either express or implied with respect to the Springer nature journal content and all parties disclaim and waive any implied warranties or warranties imposed by law, including merchantability or fitness for any particular purpose.

Please note that these rights do not automatically extend to content, data or other material published by Springer Nature that may be licensed from third parties.

If you would like to use or distribute our Springer Nature journal content to a wider audience or on a regular basis or in any other manner not expressly permitted by these Terms, please contact Springer Nature at

onlineservice@springernature.com